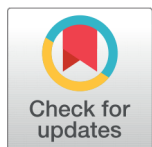


RESEARCH ARTICLE

 OPEN ACCESS

Received: 23.05.2021

Accepted: 23.06.2021

Published: 30.07.2021

Citation: Bist N, Sircar A, Yadav K (2021) Thermal zone identification by gravity data modeling using Euler deconvolution and geochemical analysis of hot springs in Saurashtra and Cambay Basins. Indian Journal of Science and Technology 14(26): 2189-2205. <https://doi.org/10.17485/IJST/v14i26.876>

* **Corresponding author.**

namrata.bist@spt.pdpu.ac.in

Funding: None

Competing Interests: None

Copyright: © 2021 Bist et al. This is an open access article distributed under the terms of the [Creative Commons Attribution License](https://creativecommons.org/licenses/by/4.0/), which permits unrestricted use, distribution, and reproduction in any medium, provided the original author and source are credited.

Published By Indian Society for Education and Environment ([iSee](https://www.isee.org/))

ISSN

Print: 0974-6846

Electronic: 0974-5645

Thermal zone identification by gravity data modeling using Euler deconvolution and geochemical analysis of hot springs in Saurashtra and Cambay Basins

Namrata Bist^{1*}, Anirbid Sircar², Kriti Yadav³

1 Assistant Professor, School of Petroleum Technology, Pandit Deendayal Petroleum University, Gandhinagar, 382007, Gujarat, India

2 Professor, School of Petroleum Technology, Pandit Deendayal Petroleum University, Gandhinagar, 382007, Gujarat, India

3 Research Scientist, School of Petroleum Technology, Pandit Deendayal Petroleum University, Gandhinagar, 382007, Gujarat, India

Abstract

Objective: This study is aimed at interpreting geochemical and geophysical data of 4 locations in Gujarat, India to understand the subsurface geothermal hotspot locations. **Methods:** CG-5 gravimeter was used to collect the gravity data. Data corrections were done to obtain a complete Bouguer anomaly. The depth of the dense bodies was calculated using Euler deconvolution. Also, the geochemical classification of physiochemical properties of geothermal spring waters of the locations was evaluated to assess their possible applications. **Findings:** In the sample region, the complete Bouguer anomaly analysis ranges between 1.99 mGal-2.23 mGal. The Euler deconvolution produced depth solutions ranging from 100 to 450 meters, which were mostly found near gravity highs, and the presence of deep structures can be deduced. These deep structures are translated as dense intruding bodies trapped by an overlying cap rock. The Geochemical analysis was done of the four samples. Based on the results of various plots such as Ternary, Durov, Piper, Stiff, the waters are graded as cationic with Na+K and anionic with Cl+SO₄. The sample waters indicate suitability for drinking and irrigation at some locations. Finding these hotspots and exploiting them is of importance for these areas which are dealing with the acute water crisis. **Novelty:** Euler deconvolution of gravity data was first time applied for subtle geothermal trap identification in Saurashtra and Cambay basins. It has been established through this study that surface manifestation of these subtle traps are the hot springs. Systematic geochemical characterization of the hot springs progressed the nascent geothermal energy research of India.

Keywords: Bouguer anomaly; Heat source; Geothermal energy; Geochemical analysis; Hot spring; water analysis

1 Introduction

Energy is the most important element for the socio-economic development of any country. However, the increased economic growth of developing nations for example India has caused accelerated consumption of energy. India is currently the fourth-largest energy consumer in the world and by 2030 it is bound to overtake the European Union as the world's third-largest energy consumer. Relying only on the nonrenewable form of energy like Coal, Oil, and Gas, etc. has major implications like environmental pollution and resource depletion. It is time to adapt the renewable form of energy such as Solar, Wind, Geothermal, etc. to support the energy needs of growing but an immensely populated country like India⁽¹⁾. Gujarat is a state in India with great contrasts and distinct coexistence of geomorphologic characteristics. The state is located on the western boundary of the Indian subcontinent. Gujarat has been gifted by Mother Nature in terms of both fossil fuels and renewable energy like Geothermal energy⁽²⁾. Exploration of this renewable resource is the first step to ascertain inherent subsurface prospects⁽²⁾. The gravity survey is a method used to calculate the gravitational anomaly based on the variation in density of the subsurface⁽³⁾. Gravimeter is used as an indirect instrument to analyze geothermal heat sources as it provides assessment about the subsurface bodies^(4,5). The earth's gravitational field in space is not constant but varies from one point to another as shown in Figure 1⁽⁶⁾. Gravimeters are used to search for oil and minerals since the 1900s. The volcanic activities, faults, and geothermal activities are mapped on the gravity map as gravity high⁽⁷⁾. Euler deconvolution can be used for gravity interpretation without adopting a geologic model of the study location⁽⁸⁾. By constructing a map of the locations and depths of the detected gravity anomaly source, the Euler deconvolution method tests the depths well as the location of the source of an anomaly within the subsurface^(8,9).

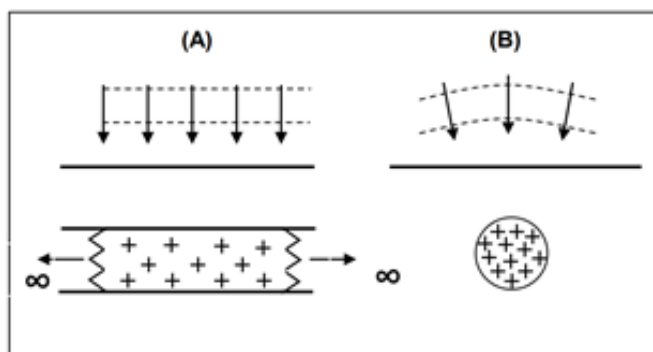


Fig 1. Effect of density variation on the generated equipotential surfaces; (A) Case of no lateral density changes, (B) Case of an anomalous, surplus density body

In this present study, four areas were selected. The gravity geophysical studies were conducted to prepare Bouguer Gravity maps and then Euler deconvolution was done to model and understand the subsurface causative bodies creating the anomaly. Along with this, geochemical prospecting was performed to assess the water quality and characteristics of the geothermal spring waters located in the study areas. Geochemistry plots like the Ternary diagram, Gibbs, Durov, Stiff chart, etc. were used in this analysis. Since certain impurities are dissolved in water during the passage, its purity is largely determined by the subsurface sources from which it flows⁽¹⁰⁾. Processes like weathering, leaching, microbial decay, etc. increase the chances of water getting impure^(11,12). The two-fold objective of this paper is to estimate subsurface structures using Euler deconvolution of Gravity Data and to characterize the hot springs in the study area to improve the use of geothermal water for practical purposes.

2 Materials and Methods

2.1 Area of study

The gravity survey was carried out in four places: A01, A02, and A03 Dholera, and one location U01 at Unai, Gujarat as seen in Figure 2, for understanding the subsurface density contrast. Dholera region is located in the Saurashtra peninsula and adjacent to the Cambay basin where Unai is located⁽²⁾. Dholera is situated at 22.2499° N latitude, 72.1934° E longitude while Unai is situated at 20.8486° N, 73.3362° E. The inland part of the Saurashtra peninsula borders the Cambay Basin on the eastern side. The major on-land part of the Saurashtra peninsula is covered by Deccan Trap volcanics of the late Cretaceous — early Paleocene age. The thick basalt sequences overspreading the Mesozoic sediments in the area make it challenging to explore the images of

the subsurface structures.



Fig 2. Area of Investigation and data acquisition points. The data acquisition points are shown by A01, A02, A03 and U01

2.2 Methodology

2.2.1 Gravity survey

A CG-5 Autograv Scintrex gravimeter was used to collect gravity data from about 150 sample locations spread over approximately 22.5 km² in Dholera and 15 km² in Unai. The measurements were repeated at the base station at the starting and end of the data acquisition every day to take care of the major drifts. For every observation point, the recording of the major parameters like the gravity value in milligal, time of observation, northing, easting, and altitude was performed. To find the Complete Bouguer Anomaly (CBA), substantial corrections to the gravity data were made; including free air, latitude, drift, landscape, and Bouguer. Gravity data interpretations aim at solving an inverse problem by using the Bouguer gravity map, translating it into geological structures. There is no standard template for gravity interpretation. There is a general sequence (Figure 3⁽⁶⁾) that should be considered in the interpretation process after the gravity data is put together and a tentative forward model of the anomaly source is made. Amplification methods might focus more on certain anomalies by deforming the anomaly pattern. Hence, these methods help in locating residual anomalies.

2.2.2 Euler Deconvolution

Euler deconvolution is a geophysical inversion process for assessing the depth and location of a causative body under the earth^(9,13,14). With the help of structural index, Euler deconvolution is a good way to figure out anomalies that come from various hidden sources⁽¹⁵⁾. As seen in equation 1, Euler deconvolution is derived from the Euler equation of homogeneity⁽¹⁾;

$$(x - x_0)T_{ZX} + (y - y_0)T_{ZY} + (z - z_0)T_{ZZ} = n(B_z - T_z) \tag{1}$$

T_z is a vertical division of the gravity anomaly source with homogeneity degree n, and (x₀,y₀,z₀) is the location of the gravity anomaly source to be calculated whose measured position of gravity is (x,y,z). Parameters (T_{ZX}, T_{ZY}, T_{ez}) are the resolute gradients in the x, y, and z directions. n is the structural index and B_z is the regional gravity value to be found out.

Since results are merely measured above observed analytic signal peaks, the window span varies depending on the scale of the phenomenon, and the concluding solution simply needs a few precise depth measurements, hence Euler deconvolution is a good choice.

In the analysis of regional gravity data interpretation, structural indices of 0.5 for dyke, 1.0 for the pipe-like model, and 2.0 for the sphere are common⁽¹⁶⁻¹⁹⁾. In Euler’s homogeneity equation, the definition of the structural index is as per Equation (2).

$$\frac{x\partial f}{\partial x} + \frac{y\partial f}{\partial y} + \frac{z\partial f}{\partial z} = nf \tag{2}$$

For gravity data processing, the term in Equation (2) is rewritten from equation (1) and can be seen in Equation (3).

$$\frac{(x - x_0)\partial T}{\partial x} + \frac{(y - y_0)\partial T}{\partial y} + \frac{(z - z_0)\partial T}{\partial z} = N(B - T) \tag{3}$$

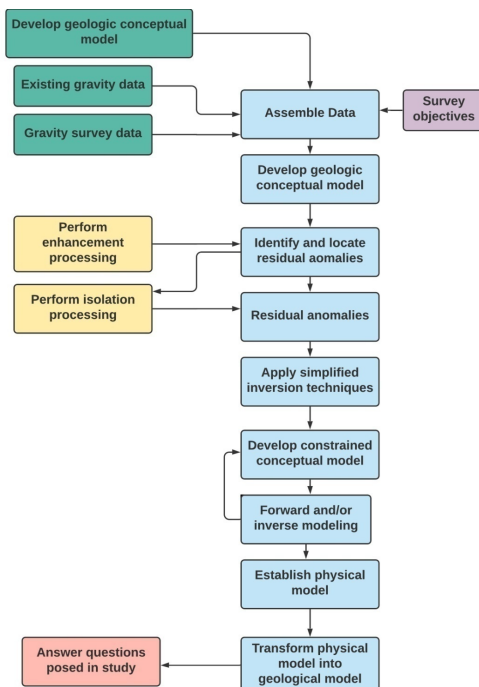


Fig 3. Flow chart depicting the components involved in the interpretation of gravity data and their inter-relationships

Where (x_0, y_0, z_0) is the position of the gravity anomaly source to be resolute, and (x, y, z) is the calculated gravity location at T. N is the structural index, and B is the regional gravity field value ⁽²⁾. For the present study, CBA data was gridded, then evaluated, with a structural index of 2, with the outputs mapped, windowed, and visualized on screen. An ultimate map was plotted with a 15% depth acceptance to assess the established solution.

2.2.3 Complete Bouguer Anomaly(CBA)

This analysis aims to assess the earth’s geothermal potential in three locations in Dholera and one location in Unai in Gujarat. Bouguer gravity data were collected from all 4 locations. Five profile lines, one perpendicular and four horizontal were used in the survey. Multiple corrections were applied after the data was obtained to convert raw gravity data to CBA. To obtain details on geothermal causative bodies, the CBA data was subjected to geographic and residual separation after density determination.

The CBA map of position A03 is seen in Figure 4. The gravity in the A03 area varies from 2 mGal to 2.23 mGal. The region can be divided into two parts, according to the contour map: (1) a high gravity value region and (2) a low gravity value region. The high gravity value part ranges from 2.17 to 2.23 mGal and the low gravity value section range from 2 to 2.16 mGal. The central portion of the map show southwest trending contours with a nose-like feature. On the south, the gravity highs are bounded by North-East trending contours. At low gravity (2.11 mGal), a four-way closure is observed, which is aided by the nose-like feature. This type of feature appears to be similar to a geothermal prospective region. The appearance of high gravity in Dholera indicates the presence of invasive bodies with a high density.

Figure 5 shows the CBA Gravity map of location A02. The map is dominated by gravity highs in the North-East direction. Bunching of contours along with pronounced gravity low is observed in the South of the map. This may be sedimentary or metamorphic rock. The region’s gravity ranges from 1.99 mGal to 2.082 mGal. The region can be divided into two parts based on the study of contour maps: (1) high gravity value region and (2) low gravity value region. The high gravity value section contains a range of values between 2.054 to 2.082 mGal, while the low gravity value between 2.054 to 2.082 mGal.

Figure 6 shows the Complete Bouguer Gravity Map of location A01. The map is dominated by gravity highs in the southeast direction. Bunching of contours along with pronounced gravity low is observed in the northwest part of the map. This may represent a sedimentary or metamorphic rock. The region’s gravity ranges from 1.99 mGal to 2.082 mGal. The region was discovered to be divided into two parts based on the study of contour maps: (1) high gravity value region and (2) low gravity value region. The gravity value of the high gravity value segment is 2.108 to 2.122 mGal, while the gravity value of the low

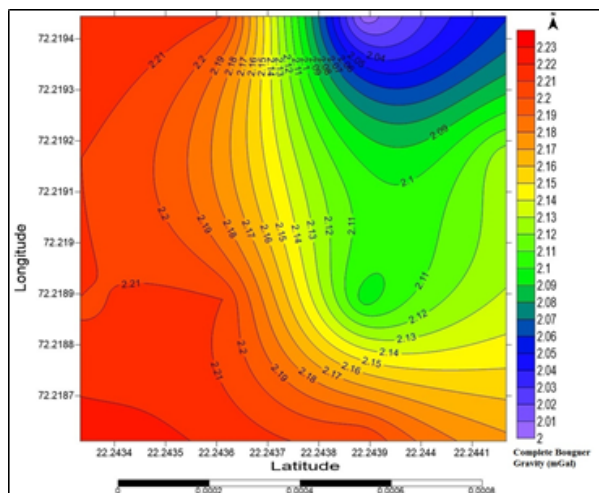


Fig 4. Complete Bouguer gravity map of A03

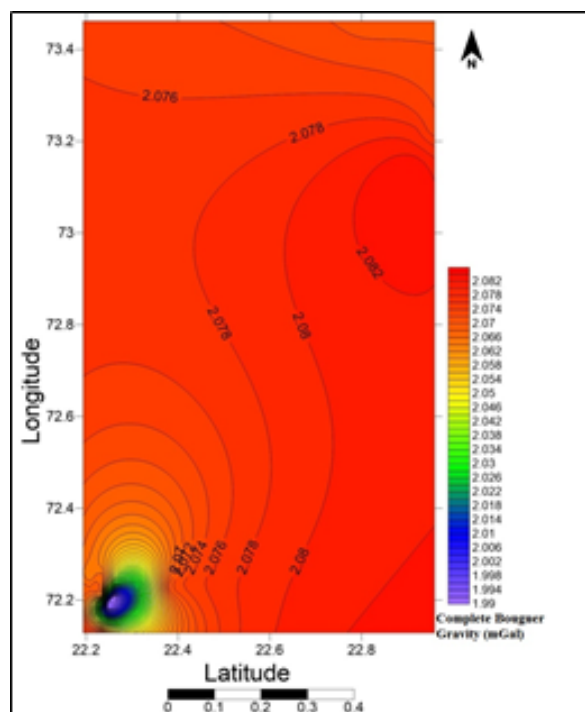


Fig 5. Complete Bouguer gravity map of A02

gravity value section is 2.08 to 2.106 mGal.

Figure 7 shows the Complete Bouguer Gravity Map of location U01. This map is very interesting. The map is dominated by gravity highs in the North East trend. The gravity highs are generally associated with sediment densification. The region's gravity ranges from 2.08 mGal to 2.101 mGal. The region was discovered to be divided into two parts based on the study of contour maps: (1) high gravity value region and (2) low gravity value region. The high gravity value section contains values ranging from 2.096 mGal to 2.101 mGal, while the low gravity value section contains values ranging from 2.08 mGal to 2.094 mGal. A prominent structural feature is visible at the South-West corner of the map resembling an antiform. Sudden changes from gravity low to gravity high occur at the South-East corner of the map depicts a fault boundary.

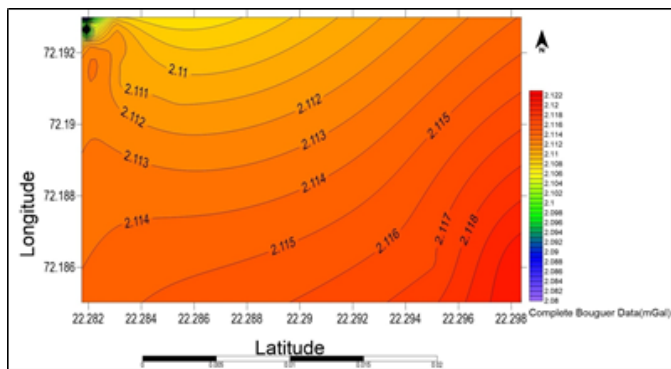


Fig 6. Complete Bouguer gravity map of A01

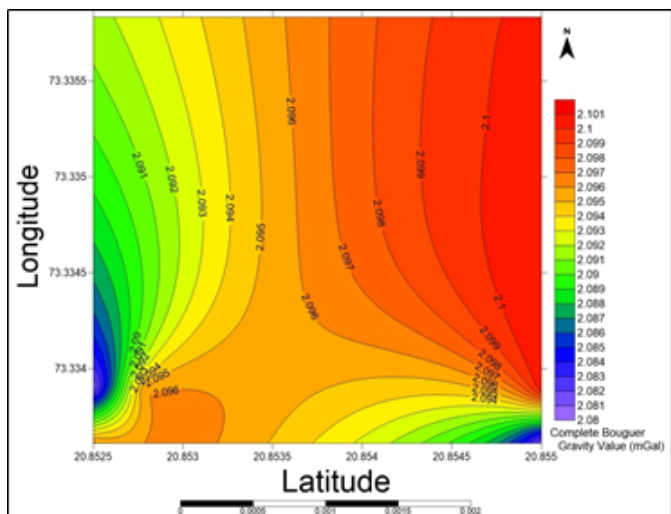


Fig 7. Bouguer gravity map of U01

2.2.4 Regional and Residual Bouguer Anomaly

A Bouguer anomaly map normally shows gravity variations that consist of two components which are Long-wavelength variation also known as regional gravity and Short-wavelength variation referred to as residual gravity or residuals. The former component reflects deep geological anomalies which are of large and regional extent, while the latter variations reflect shallow geological anomalies which are of restricted or local nature. The residual gravity is obtained by removing the regional component from the Bouguer map. The first step in interpreting Bouguer gravity data is the isolation of the residual anomalies by removing the regional anomaly from the original Bouguer anomaly map. The technique used in this study is polynomial fitting. The method of polynomial fitting assumes that the regional field can be approximated by a low-order polynomial surface. In this method, the Bouguer gravity profile (or map) is expressed by a low-order polynomial as shown in equation 5 and 6:

$$g(X) = C_0 + C_1x + C_2X^2 + C_3x^3 + C_4x^4 + C_5x^5 \dots \text{(for a profile)} \tag{5}$$

$$g(X,Y) = C_0 + C_1x + C_2y + C_3xy + C_4x^2 + C_5y^2 + \dots \text{(for a map)} \tag{6}$$

The coefficients (C0, C1, C2...) are determined by a least-squares analysis. This will express the regional gravity which is subtracted from the Bouguer values to obtain the residual.

The residual map is generated after the regional surface is subtracted from the original map. Regional and residual separation of the earth is a successful method of maintaining a connection between geological formations and gravity. A regional-residual investigation was conducted along multiple profiles to assess the residual Bouguer gravity plots. The residual gravity plots improved the properties of the area of interest in all of the sample regions. The method of Regional residual separation across

one section is shown in Figure 8. A similar method was applied to all the sections and subsequent Residual maps were prepared for the study areas.

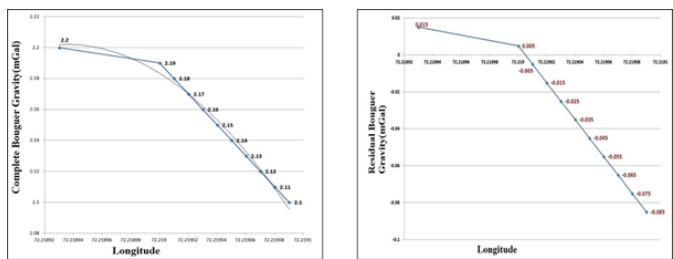


Fig 8. A) Representation of Bouguer anomaly across one of the section B) Residual anomaly from CBA

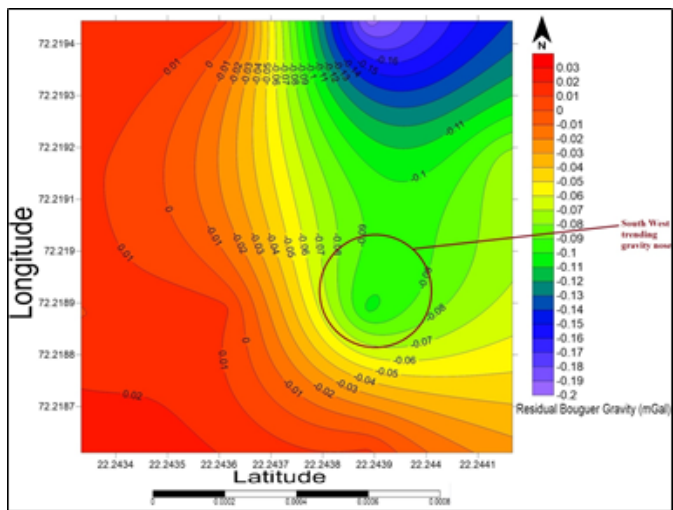


Fig 9. Residual Bouguer gravity map of A03

Figure 9 shows the Residual Bouguer gravity map of location A03. The residual gravity values of the A03 region vary from -0.2 mGal to 0.03 mGal. The central portion of the map shows southwest trending contours with a nose-like feature. The gravity highs are bounded on the south by North-East trending contours. At low gravity (0.09 mGal), a four-way closure is also observed, which is accompanied by the nosing function. This sort of feature looks a lot like a geothermal potential field. The presence of high gravity in Dholera signals the presence of high-density invasive bodies.

Figure 10 shows the Residual Bouguer Gravity Map of location A02. The map is dominated by gravity highs in the North-East direction. In the south of the map, there is a clustering of contours as well as a pronounced gravity low. This may represent a sedimentary or metamorphic rock. The residual gravity values of the region vary from -0.015 mGal to 0.077 mGal. The presence of three faults can be observed in the southwest corner of the map. A location of the possible geothermal hot spot can be deduced out of this location.

Figure 11 shows the Residual Bouguer Gravity Map of location A01. The map is dominated by gravity highs in the southeast direction. A prominent Bunching of contours along with pronounced gravity low is observed in the northwest part of the map. This may represent a sedimentary or metamorphic rock. The residual gravity values of the region vary from -0.026 mGal to 0.016 mGal.

Figure 12 shows a Residual Bouguer Gravity Map of location U01. The map is dominated by gravity highs in the North-East direction. A prominent Bunching of contours along with pronounced gravity low is observed in the northwest part of the map. This may represent a sedimentary or metamorphic rock. The residual gravity values of the region vary from -0.015 mGal to 0.006 mGal. Sudden changes from gravity low to gravity high occur at the South-East corner of the map depicting a fault boundary.

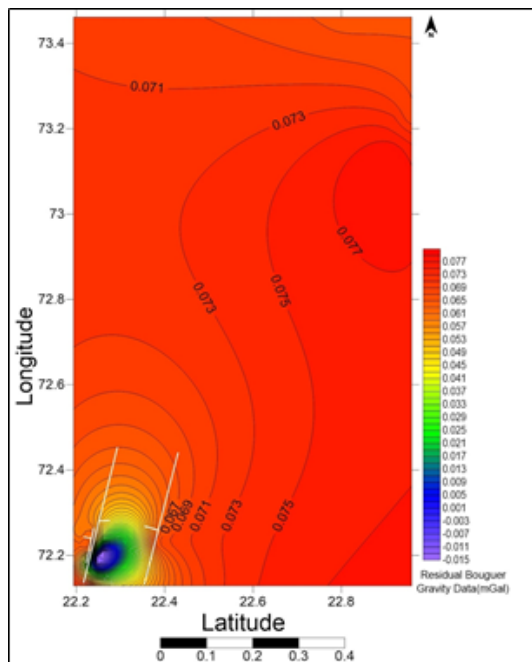


Fig 10. Residual Bouguer gravity map of A02

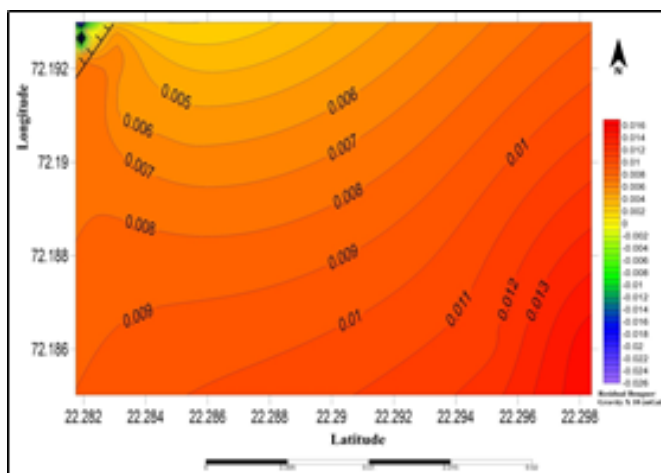


Fig 11. Residual Bouguer gravity map of A01

2.2.5 Euler Deconvolution: Results and Discussion

At depths of 100 m - 150 m, 150 m - 250 m, 250 m - 350 m, 350 m - 450 m, and greater than 450 m, the Euler deconvolution provided five solutions, all of which occurred nearly at the same position on gravity highs. Each location is discussed in brief as per the following:

As shown in Figure 13, the Euler deconvolution of the A03 location generated more than five solution depths. The deepest Euler solution is found in the location's south-western corner, at 465 m deep and magnitude of gravity 0.01 mGal. This is likely hot, dense material trapped in the crust from the earth's mantle. At a depth of 103 m, the shallowest depth solution with a gravity amplitude of 0.01 mGal can be found. Many Euler solution depths are displayed extending all over the high portions of the map in the Western most margins with a depth ranging from 463 m - 110 m.

Figure 14 shows the Euler deconvolution of the A02 location. The deepest Euler solution is found in the location's south-western corner, at 590 m depth and magnitude of gravity 0.067 mGal. This is likely hot, dense material trapped in the crust from

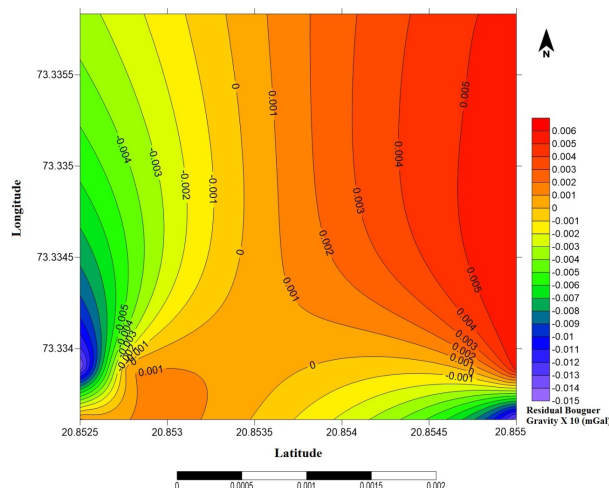


Fig 12. Residual Bouguer gravity map of U01

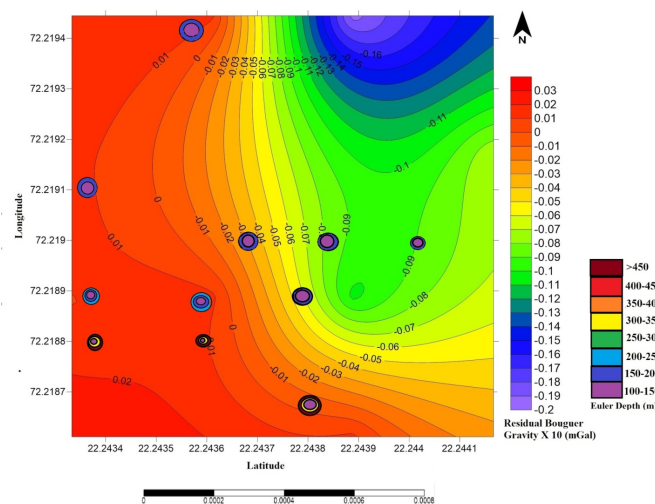


Fig 13. Located Euler deconvolution results for A03

the earth’s mantle. At a depth of 110 m, the shallowest depth solution, with a gravity amplitude of 0.067 mGal, can be found. Many Euler solution depths are displayed extending all over the high portions of the map in the NE-SW margins with a depth ranging from 590 m – 110 m.

Figure 15 shows the Euler deconvolution of the A01 location. The deepest Euler solution is found in the location’s south-western corner, at 540 m depth and magnitude of gravity -0.025 mGal. The shallowest depth solution, with high gravity amplitude of 0.012 mGal, can be found at a depth of 108 m. Many Euler solution depths are displayed extending all over the high portions of the map in the NW-SE margins with a depth ranging from 540 m – 108 m.

Figure 16 shows the Euler deconvolution of the U01 location. The deepest Euler solution is found in the location’s south-western corner, at 536 m depth and magnitude of gravity -0.0141 mGal. The shallowest depth solution, with high gravity amplitude of 0.0045 mGal, can be found at a depth of 134 m. Many Euler solution depths are displayed extending all over the map in the NE-SW margins with a depth ranging from 536 m – 134 m.

2.2.6 Geochemical data of surface hot springs

The geothermal waters are a valuable natural source for understanding the geothermal productivity of an area. They also are useful for societal and industrial uses. In this study, four geothermal hot spring water samples were collected from A01, A02,

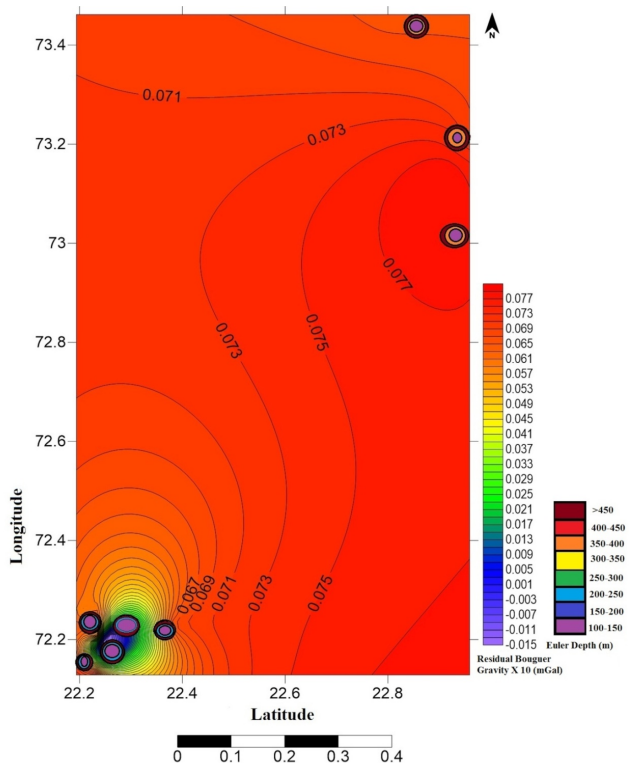


Fig 14. Located Euler deconvolution results for A02

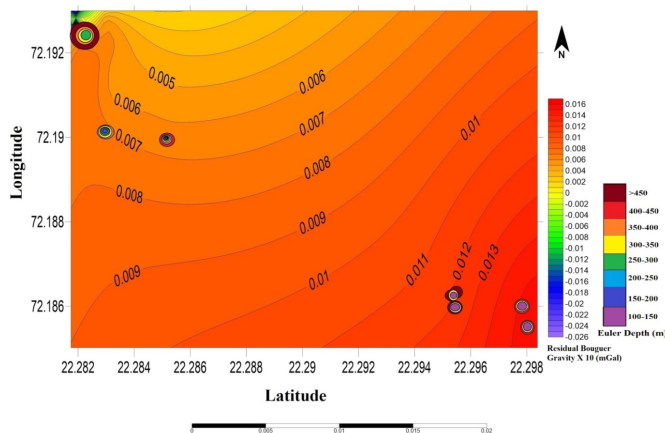


Fig 15. Located Euler deconvolution results for A01

A03 locations in Dholera and U01 in Unai. The water samples were collected in 700-milliliter bottles for the determination of parameters as shown in Table 1 . Geochemical prospecting was performed to assess the water quality and characteristics of the waters. The physical and chemical properties like color, taste, pH, and conductivity were analyzed as shown in Table 2.

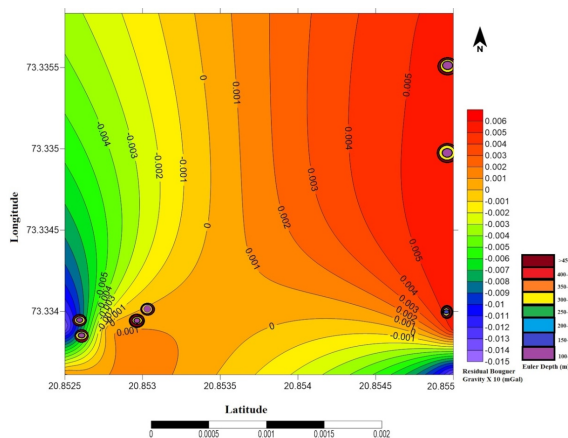


Fig 16. Located Euler deconvolution results for U01

Table 1. Concentration of cations and anion in geothermal spring water

S.No.	Place	Ca	Mg	Na	K	CO ₃ mg/l	HCO ₃ mg/l	Cl mg/l	SO ₄ mg/l
1	A01,Dholera	110	26.05	2600	15	0	70	3800	10.5
2	A02, Dholera	130.5	30	2000	19	0	65	3500	9.01
3	A03, Dholera	98.24	21.2	1800	8	0	38	2100	11
4	Unai	50	7	310	11	4.1	35	550	50.35

Table 2. Thermal water sample physical parameters

Sr. No	Location	Odour	pH	Conductivity Ms/cm	Salinity mg/l	TDS mg/l	CO ₃ Hardness mg/l	Electrical Conductivity
1	A01,Dholera	Odourless	8.0	8100	6100	7357	99	10980
2	A02,Dholera	Odourless	8.19	8390	6300	7100	135	10510
3	A03,Dholera	Odourless	7.9	7990	6850	4800	150	8900
4	Unai	Odourless	7.5	1800	600	890	90	1900

3 Tables

Ternary Diagram

The ternary diagram is used to illustrate the proportion of main ions found in geothermal spring water⁽¹⁶⁾. For creating phase diagrams and depicting composition in a two-dimensional graph ternary diagrams can be used⁽²⁰⁾. The ternary diagram for cations is seen in Figure 17 and is dominated by Na. The emergence of high Na levels may be a factor in the high salinity levels. The ternary diagram for anions is shown in Figure 18 and is occupied by Cl ions. It’s also possible to deduce that all four samples were mature.

Schoeller Diagram

In Schoeller’s chart, major cations and anions are plotted on the horizontal axis having equal divisions and the vertical scale is the logarithmic scale of an equal concentration of these ions. To envisage the relationship between two ions points are connected by polyline and the slope of the line between two ions can be equated with other samples⁽²¹⁾. As seen in Figure 19, as compared to the other samples, the water sample from A01 has the largest concentration of K, Mg, Ca, Na, Cl, SO₄, and HCO₃. The SO₄ concentrations in A02, A03, and U01 are at low levels, suggesting that volcanic gases are combined with thermal spring waters⁽²²⁾.

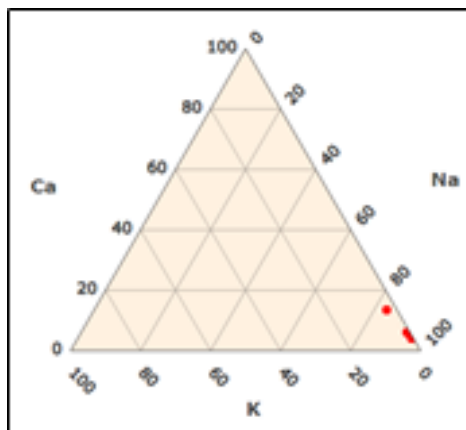


Fig 17. Ternary diagram depicting cation (Na-Mg-K) concentration

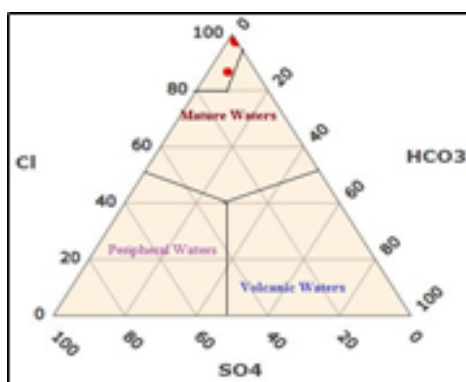


Fig 18. Ternary diagram depicting anion (Cl-SO4-HCO3) concentration

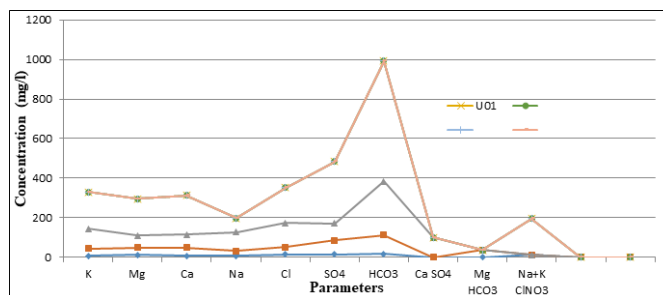


Fig 19. Schoeller Diagram

Piper Plot

The Piper chart for water chemistry is made up of two ternary charts that display the normalized milliequivalent percent of anions and cations, respectively. Plotting of major cations and anions in this tri-linear diagram can give an understanding of the hydrochemical evolution of hot spring water. The Piper plot contains two split tri-linear plots they are cations and anions respectively comparative concentration of each other⁽²¹⁾. Out of four locations, three locations in Dholera show high Cl concentrations. In the bottom left triangle of Figure 20, the amounts of cations such as calcium, magnesium, sodium, and potassium are seen.

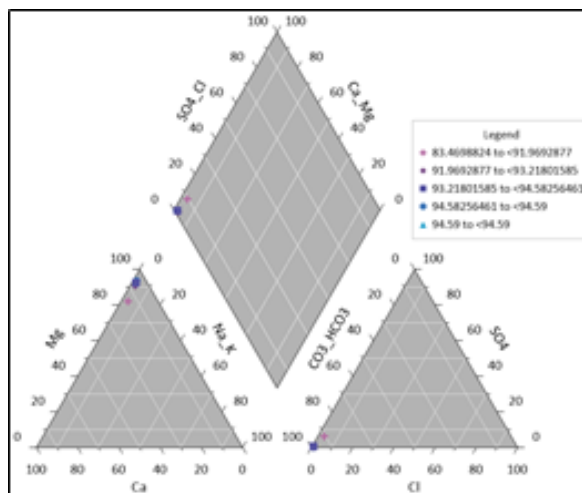


Fig 20. Piper chart for the sample Geothermal waters

Extended Durov Diagram

The Durov plot is used to visualize the cation and anion concentrations graphically and to understand the hydrochemical processes of water. The extended Durov plot can also be used to represent the sample’s total dissolved solids (TDS) and pH. A pH plot is adjoined to the bottom and a TDS plot is added to the right side of the diagram in the extended Durov plot. This diagram is extremely helpful in comprehending the properties of undesirable products that can alter groundwater content. Figure 21 displays the anions and cations concentrations in two ternary diagrams. The water samples were observed to have high ion concentrations ranging from 1013.35 to 4076.44.

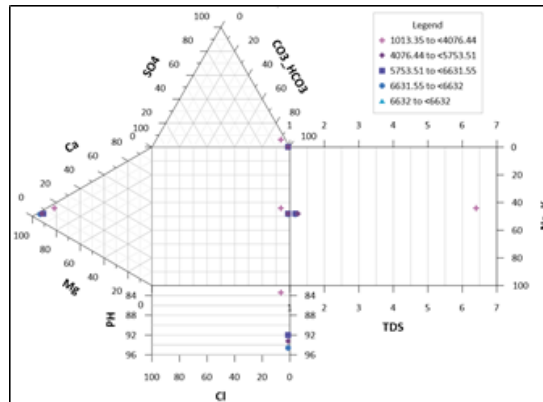


Fig 21. Cations and Anions in Geothermal Water represented by Extended Durov Diagram

Stiff Diagram

The Stiff diagram is a graphical demonstration of chemical analysis and major ion composition of water. Intending to create a quick visual assessment of water from diverse sources, stiff diagrams are useful⁽²³⁾. Figure 22 represents the stiff diagram series for all four sites, with anions on the right side and cations on the left side of each line.

Wilcox Log

The analysis of groundwater’s applicability for irrigation rationale can be performed by the Wilcox diagram. The Wilcox diagram has shown A01, A02, and A03 samples unsuitable for irrigation or drinking purposes but sample U01 is found good for irrigation and drinking.

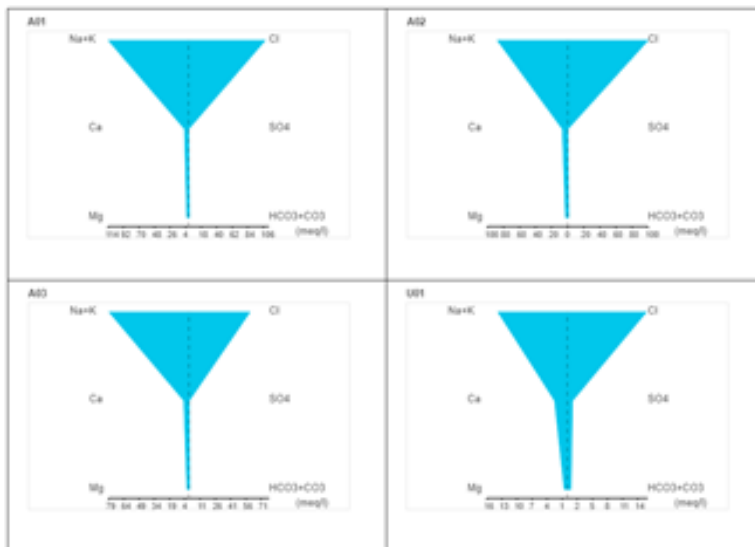


Fig 22. Stiff Diagrams of the four Thermal Springs sites

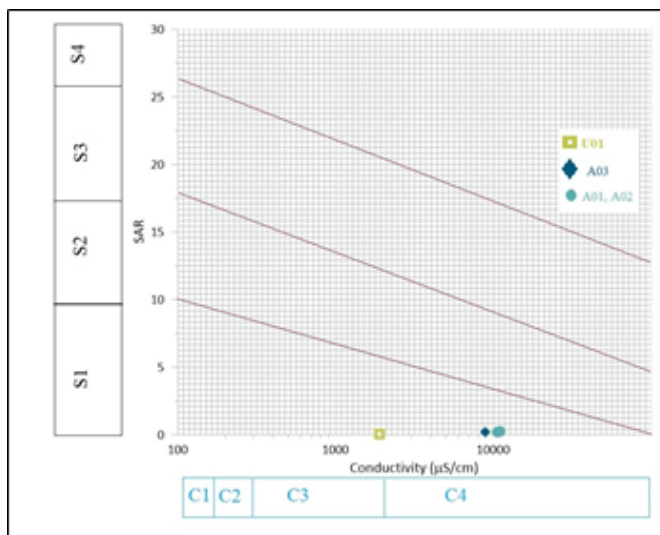


Fig 23. Wilcox log plot of various Thermal Springs sites in Gujarat

As shown in Figure 23, the A01, A02, and A03 samples are within the S1-C4 range and indicate useful for irrigation but unsuitable for drinking. Whereas the U01 sample is within the S1-C3 range and indicates suitability for usages in drinking and irrigation.

Gibbs plot

Gibbs plot shows the influence of the main leading processes like evaporation, precipitation, and water-rock interaction on water’s chemical composition. In the Gibbs plot, $Na/(Ca+Na)$ ratios are plotted on X-axis against TDS (Salinity) on the Y-axis⁽²⁴⁾.

The Gibbs diagram shows rock dominance or rock-forming minerals. None of the samples from both diagrams in Figure 24 shows precipitation dominance. The rock water interference present in the area may be the factor for controlling the geochemistry of the area^(25,26).

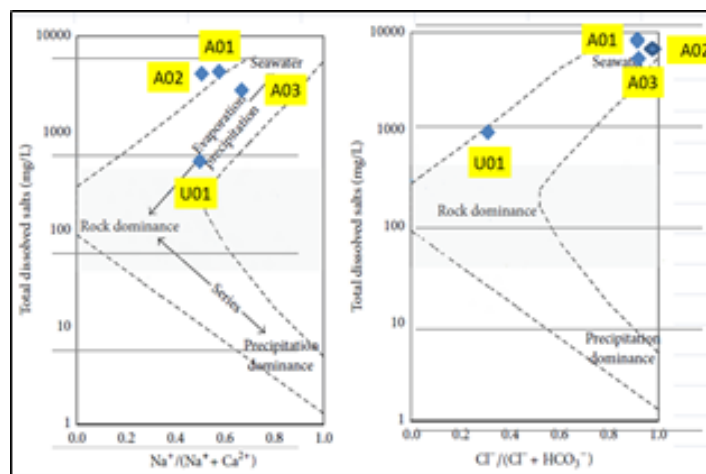


Fig 24. Gibbs plot of various Thermal Springs sites in Gujarat

4 Results and Discussion

The present study investigated four locations for the presence of Geothermal hotspots. This was done by gathering gravity data and then modeling the gravity data by Euler deconvolution to find subsurface causative bodies creating gravity anomalies. By Euler's deconvolution, it was found that all the four locations had causative bodies at deep locations. These may be hot, dense mantle embedded deep within the earth's crust. The depth ranges of the causative bodies have been found from 463 m – 110 m in the A03 location, 590 m – 110 m in the A02 location, 540 m – 108 m in A01, and 536 m – 134 m in the U01 location. The shallowest and deepest Euler depths were found at the same gravity values. These studies ascertain the presence of hot geothermal sources in the locations. These locations may be drilled for exploiting the geothermal water for a variety of usages such as electricity production, balneology, honey processing, etc. The hot intruding bodies could be stuck under an impervious sedimentary caprock, stopping them from reaching shallow depths^(19,27). Subsurface faults may be releasing water from a variety of reservoirs into the geothermal heat source^(28,29). Geothermal waters are classified as Na+K-Cl+SO₄ based on the Ternary, Piper, Durov, and Stiff Diagrams. In all four samples, the carbonate and bicarbonate concentrations are low. The water is thought to have been meteoric in origin, having seeped to depths and been influenced by sedimentary rocks with underlying igneous formations⁽³⁰⁾. Since water might have come into contact with minerals like mica and feldspars, the presence of Na, Cl, and K can be inferred⁽³¹⁾. In the geothermal waters of Dholera, high salinity values of up to 6000mg/l have been reported. These waters are thought to have formed by mixing with granitic basements at depth^(32,33). Unai's sample has low salinity, and the TDS values follow the same pattern. CO₃ levels are minimal in all of the samples, and anions such as SO₄ and Cl dominate the compositions. Fluoride amounts suggest that thermal waters interacted with the granitic basement under the Mesozoic sedimentary spread. Fluoride is absorbed into the water by these formations^(21,34). The cation and anion data points towards the presence of meteoric signature in the waters and the waters seeped to the surface after attaining boiling point due to meteoric activity^(35,36). Similar studies based on the isotope data of the region points towards the meteoric origin of the waters⁽¹⁶⁾.

5 Conclusion

To create a balance between energy demand and supply, continuous efforts in the exploration of renewable energy are required. Geothermal energy has shown great advantages over other renewable energies as it is present 365 days a year. The literature has shown great scope for Geothermal energy in Gujarat, India. The present study analyzed gravity geophysical exploration and geochemical analysis of samples from four locations viz. A01, A02, and A03 in Dholera and U01 in Unai. The study tried to analyze the subsurface causative bodies for the gravitational anomalies in the locations. By Euler deconvolution, all the four locations were analyzed with the presence of causative bodies at deep locations. Euler deconvolution of gravity data was first time applied for subtle geothermal trap identification in Saurashtra and Cambay basins. It has been established through this study that the surface manifestation of these subtle traps is the hot springs. It is derived that these locations may have a hot and dense mantle that is enclosed deeply in the crust. The presence of a hot geothermal source can be ascertained in the four locations. The hot intruding bodies could be stuck under an impervious sedimentary caprock, stopping them from reaching shallow depths. Subsurface faults may be releasing water from a variety of reservoirs into the geothermal heat source. When trapped

underground, this water becomes hot and migrates through geological systems, forming a geothermal reservoir. Along with the geophysical study, the geochemical analysis was also performed to ascertain the usability of these hot springs in locations A01, A02, A03, and U01. Systematic geochemical characterization of the hot springs progressed the nascent geothermal energy research of India. Out of the four samples, U01 and A01 are found fit for drinking and irrigation purposes. Samples A02 and A03 although are not fit for drinking, but maybe utilized for irrigation methods. However, with pretreatment, these locations could also be utilized for drinking purposes.

Acknowledgment

The authors gratefully acknowledge Pandit Deendayal Petroleum University and the Government of Gujarat for providing facilities to carry out this research.

References

- 1) Bist N, Sircar A, Yadav K. Holistic review of hybrid renewable energy in circular economy for valorization and management. *Environmental Technology & Innovation*. 2020;20(101054). Available from: <https://dx.doi.org/10.1016/j.eti.2020.101054>.
- 2) Sircar A, Shah M, Sahajpal S, Vaidya D, Dhale S, Chaudhary A. Geothermal exploration in Gujarat: case study from Dholera. *Geothermal Energy*. 2015;3:1–25. Available from: <https://dx.doi.org/10.1186/s40517-015-0041-5>.
- 3) Kearey P, Brooks M, Hill I. An introduction to geophysical exploration. John Wiley & Sons. 2002. Available from: <https://www.wiley.com/en-us/An+Introduction+to+Geophysical+Exploration%2C+3rd+Edition-p-9780632049295>.
- 4) Lúdvik SG. Geophysical methods used in geothermal exploration. Short Course on Surface Exploration for Geothermal Resources. . Available from: <https://orkustofnun.is/gogn/unu-gtp-sc/UNU-GTP-SC-09-05.pdf>.
- 5) Yadav K, Sircar A. Integrated 2D joint inversion models of gravity, magnetic, and MT for geothermal potentials: a case study from Gujarat, India. *Modeling Earth Systems and Environment*. 2019;5:963–983. Available from: <https://dx.doi.org/10.1007/s40808-019-00582-2>.
- 6) Alsadi HN, Baban EN. Introduction to Gravity Exploration Method. 2014. Available from: https://www.researchgate.net/profile/Ezadin-Baban/publication/282735037_Introduction_to_gravity_exploration_method/links/561ac40608ae78721f9f8d46/Introduction-to-gravity-exploration-method.pdf.
- 7) Nicholas M, UNU-GTP, GDC and KenGen. Application of geophysical methods to geothermal energy exploration in Kenya. Kenya. 2010. Available from: <https://orkustofnun.is/gogn/unu-gtp-sc/UNU-GTP-SC-13-0405A.pdf>.
- 8) Dewangan P, Ramprasad T, Ramana MV, Desa M, Shailaja B. Automatic Interpretation of Magnetic Data Using Euler Deconvolution with Nonlinear Background. *Pure and Applied Geophysics*. 2007;164:2359–2372. Available from: <https://dx.doi.org/10.1007/s00024-007-0264-x>.
- 9) ER N, JG G, WJ A. Geophysical Investigation of Geothermal Potential of the Gilgil Area Nakuru County, Kenya Using Gravity. *Journal of Geology & Geophysics*. 2017;06(02). Available from: <https://dx.doi.org/10.4172/2381-8719.1000278>.
- 10) Fard MJ, Amanipoor H, Battaleb-Looie S, Ghanemi K. Evaluation of effect factors on water quality of Karun River in downstream and lake of the Gotvand-e-Olya Dam (SW Iran). *Applied Water Science*. 2019;9(7):1–4. Available from: <https://dx.doi.org/10.1007/s13201-019-1040-7>.
- 11) Nagaraju A, Kumar KS, Thejaswi A. Assessment of groundwater quality for irrigation: a case study from Bandalamottu lead mining area, Guntur District, Andhra Pradesh, South India. *Applied Water Science*. 2014;4(4):385–396. Available from: <https://dx.doi.org/10.1007/s13201-014-0154-1>.
- 12) Rahimi L, Amanipoor H, Battaleb-Looie S. Effect of salinity of irrigation water on soil properties (abadan plain, SW Iran). *Geocarto International*. 2019;p. 1–20. Available from: <https://doi.org/10.1080/10106049.2019.1678678>.
- 13) Keating PB. Weighted Euler deconvolution of gravity data. *Geophysics*. 1998;63(5):1595–1603. Available from: <https://dx.doi.org/10.1190/1.1444456>.
- 14) Pan Q, Liu D, Feng S, Feng M, Fang H. Euler deconvolution of the analytic signals of the gravity gradient tensor for the horizontal pipeline of finite length by horizontal cylinder calculation. *Journal of Geophysics and Engineering*. 2017;14(2):316–330. Available from: <https://dx.doi.org/10.1088/1742-2140/aa5a23>.
- 15) Dawi MGE, Tianyou L, Hui S, Dapeng L. Depth Estimation of 2-D Magnetic Anomalous Sources by Using Euler Deconvolution Method. *American Journal of Applied Sciences*. 2004;1(3):209–214. Available from: <https://dx.doi.org/10.3844/ajassp.2004.209.214>.
- 16) Yadav K, Sircar A, Jani D, Bist N, Nirantare A, Mali N, et al. Geochemical characterization of geothermal spring waters occurring in Gujarat, India. *International Journal of Energy and Water Resources*. 2021;4:1–4. Available from: <https://dx.doi.org/10.1007/s42108-020-00111-3>.
- 17) Ghosh GK. Interpretation of Gravity Data using 3D Euler Deconvolution, Tilt Angle, Horizontal Tilt Angle and Source Edge Approximation of the North-West Himalaya. *Acta Geophysica*. 2016;64(4):1112–1138. Available from: [10.1515/acgeo-2016-0042](https://doi.org/10.1515/acgeo-2016-0042).
- 18) Daud Y, Sulisty A, Fahmi F, Nuqramadha WA, Fitrianita, Sesesega RS, et al. First horizontal derivative and Euler Deconvolution in application for reconstructing structural signature over the Blawan-Ijen Geothermal area. *IOP Conference Series: Earth and Environmental Science*. 2019;254(012008). Available from: <https://dx.doi.org/10.1088/1755-1315/254/1/012008>.
- 19) Eshani AS, Osagie AU, Ismail NA, Ghanush HB. Analysis of gravity and aeromagnetic data to determine structural trend and basement depth beneath the Ajdabiya Trough in northeastern Libya. *SN Applied Sciences*. 2021;3(2):1–15. Available from: <https://dx.doi.org/10.1007/s42452-021-04263-7>.
- 20) Shyamala G, Jeyanthi J. Application of Integrated Hydrochemical Model and Cluster Analysis in Assessing Groundwater Quality. *International Journal of Ecology & Development*. 2016;31(4):34–45.
- 21) Shah M, Sircar A, Shaikh N, Patel K, Thakar V, Sharma D, et al. Groundwater analysis of Dholera geothermal field, Gujarat, India for suitable applications. *Groundwater for Sustainable Development*. 2018;7:143–156. Available from: <https://dx.doi.org/10.1016/j.gsd.2018.05.002>.
- 22) Shah M, Sircar A, Shaikh N, Patel K, Sharma D, Vaidya D. Comprehensive geochemical/hydrochemical and geo-thermometry analysis of Unai geothermal field, Gujarat, India. *Acta Geochimica*. 2019;38(1):145–158. Available from: <https://dx.doi.org/10.1007/s11631-018-0291-6>.
- 23) Arthur H. Water quality data: analysis and interpretation. CRC press. 1995. Available from: <https://www.taylorfrancis.com/books/mono/10.1201/9780203734117/water-quality-data-arthur-hounslow>.
- 24) Marandi A, Shand P. Groundwater chemistry and the Gibbs Diagram. *Applied Geochemistry*. 2018;97:209–212. Available from: <https://dx.doi.org/10.1016/j.apgeochem.2018.07.009>.

- 25) Alam F. Evaluation of hydrogeochemical parameters of groundwater for suitability of domestic and irrigational purposes: a case study from central Ganga Plain, India. *Arabian Journal of Geosciences*. 2014;7(10):4121–4131. Available from: <https://dx.doi.org/10.1007/s12517-013-1055-6>.
- 26) Raju NJ, Shukla UK, Ram P. Hydrogeochemistry for the assessment of groundwater quality in Varanasi: a fast-urbanizing center in Uttar Pradesh, India. In: *Environmental Monitoring and Assessment*; vol. 173. Uttar Pradesh, India. Springer Science and Business Media LLC. 2011;p. 279–300. Available from: <https://dx.doi.org/10.1007/s10661-010-1387-6>. doi:10.1007/s10661-010-1387-6.
- 27) Perdana T, Satria C, Bing-Chen H, Ann RT, Amber T. Geothermal Resource Evaluation of the Tatun Volcano Group (TVG) Area, Taiwan. Taiwan. . Available from: <https://pangea.stanford.edu/ERE/db/GeoConf/papers/SGW/2021/Perdana.pdf>.
- 28) Zhou L, Zhang Y, Luo Y, Lei Y, Hao S. The Zhacang thermal field, Qinghai Province, China: its geology, geophysics, chemistry, and conceptual model. *Arabian Journal of Geosciences*. 2021;14(8):1–8. Available from: <https://dx.doi.org/10.1007/s12517-021-07040-3>.
- 29) Syamsu RM, Sibarani C. Reservoir identification at Dieng geothermal field using 3D inversion modeling of gravity data. *Presented at InJournal of Physics: Conference Series 2021*. 12083. Available from: <https://iopscience.iop.org/article/10.1088/1742-6596/1816/1/012083/pdf>.
- 30) Brehme M, Giese R, Suherlina L, Kamah Y. Geothermal sweetspots identified in a volcanic lake integrating bathymetry and fluid chemistry. *Scientific Reports*. 2019;9:1–1. Available from: <https://dx.doi.org/10.1038/s41598-019-52638-z>.
- 31) Stefánsson A, Arnórsson S. Feldspar saturation state in natural waters. *Geochimica et Cosmochimica Acta*. 2000;64(15):2567–2584. Available from: [https://dx.doi.org/10.1016/s0016-7037\(00\)00392-6](https://dx.doi.org/10.1016/s0016-7037(00)00392-6).
- 32) Danda N, Rao CK, Kumar A. Geoelectric structure of northern Cambay rift basin from magnetotelluric data. *Earth, Planets and Space*. 2017;69:1–4. Available from: <https://dx.doi.org/10.1186/s40623-017-0725-0>.
- 33) Sureshjani MK, Amanipoor H, Battaleb-Looie S. The Effects of Industrial Wastewater on Groundwater Quality of the Boroujen Aquifer, Southwest Iran. *Natural Resources Research*. 2020;29:3719–3741. Available from: <https://dx.doi.org/10.1007/s11053-020-09665-9>.
- 34) Frančičković-Bilinski S, Sakan S. Geochemistry of Water and Sediment. *Water*. 2021;13:693. Available from: <https://dx.doi.org/10.3390/w13050693>.
- 35) Talabi AO, Tijani MN. Hydrochemical and stable isotopic characterization of shallow groundwater system in the crystalline basement terrain of Ekiti area, southwestern Nigeria. *Applied Water Science*. 2013;3:229–245. Available from: <https://dx.doi.org/10.1007/s13201-013-0076-3>.
- 36) Naidu S, Gupta G, Singh R, Tahama K, Erram VC. Hydrogeochemical Processes Regulating the Groundwater Quality and its Suitability for Drinking and Irrigation Purpose in Parts of Coastal Sindhudurg District, Maharashtra. *Journal of the Geological Society of India*. 2021;97(2):173–185. Available from: <https://dx.doi.org/10.1007/s12594-021-1649-7>.